AIAA 98–0170

Aerothermal Heating Predictions for Mars Microprobe

R. A. Mitcheltree, M. DiFulvio, T. J. Horvath, and R. D. Braun
NASA Langley Research Center, Hampton, Virginia

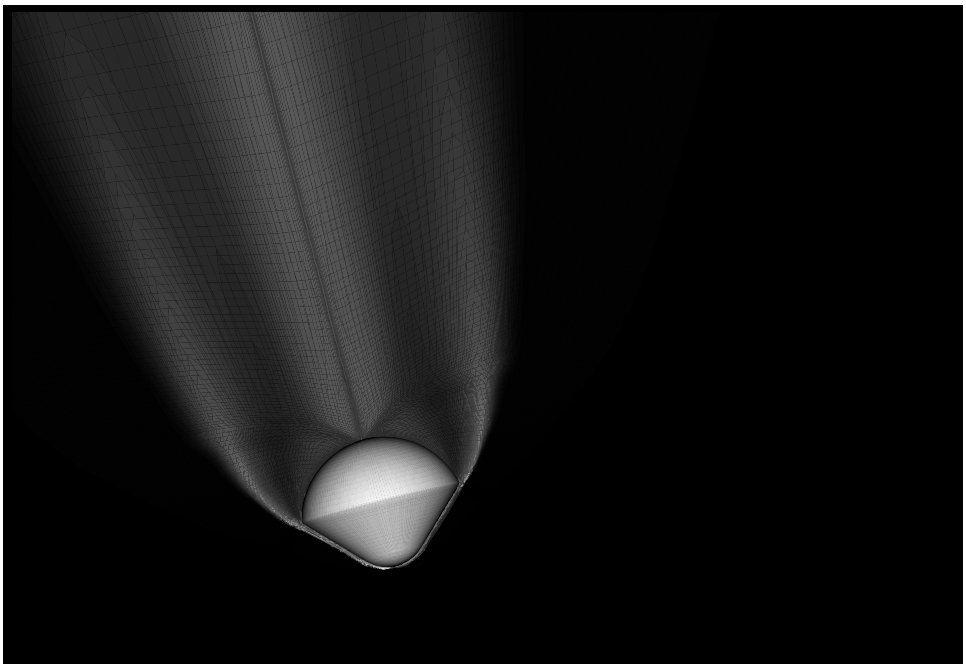

36th Aerospace Sciences Meeting
January 12–15, 1998/Reno, NV

Aerothermal Heating Predictions for Mars Microprobe

R. A. Mitcheltree*, M. DiFulvio†, T. J. Horvath‡, and R. D. Braun§
NASA Langley Research Center, Hampton, Virginia

A combination of computational predictions and experimental measurements of the aerothermal heating expected on the two Mars Microprobes during their entry to Mars are presented. The maximum, non-ablating, heating rate at the vehicle's stagnation point (at $\alpha = 0^0$)is predicted for an undershoot trajectory to be 194 W/cm^2 with associated stagnation point pressure of 0.064 atm. Maximum stagnation point pressure occurs later during the undershoot trajectory and is 0.094 atm. From computations at seven overshoot-trajectory points, the maximum heat load expected at the stagnation point is near 8800 J/cm^2. Heat rates and heat loads on the vehicle's afterbody are much lower than the forebody. At zero degree angle-of-attack, heating over much of the hemispherical afterbody is predicted to be less than 2 percent of the stagnation point value. Good qualitative agreement is demonstrated for forebody and afterbody heating between CFD calculations at Mars entry conditions and experimental thermographic phosphor measurements from the Langley 20-Inch Mach 6 Air Tunnel. A novel approach which incorporates six degree-of-freedom trajectory simulations to perform a statistical estimate of the effect of angle-of-attack, and other off-nominal conditions, on heating is included.

Nomenclature

B = Ballistic coefficient, kg/m^2
C_h = heat transfer coefficient
M = Mach number
P = pressure, atm
q = heat rate, W/cm^2
R_n = nose radius, m
s = surface distance from geometric stagnation point, m
t = independent variable time, s
V = velocity, m/s
x, z = independent spatial dimensions, m
α = angle-of-attack, deg
β = side-slip angle, deg
ρ = density, kg/m^3
σ = standard deviation

Introduction

When the Mars Surveyor 98 Lander is launched in January of 1999, it will transport not only its own lander to Mars, but two small soil penetrators. These two Mars Microprobes[1] are the second of the Deep Space missions from NASA's New Millennium Program Office. Upon arrival at Mars, the penetrators will be released from the cruise stage and begin a free fall to the surface. This paper focuses on predicting the convective heating which the aeroshells will encounter during the hypersonic portion of that Mars entry. Knowledge of the expected heating is necessary to design forebody and afterbody Thermal Protection Systems (TPS).

Both Computational Fluid Dynamics (CFD) predictions and experimental measurements are presented. The quantitative analysis focuses on computational predictions for heating at zero degrees angle-of-attack. Solutions are generated at the estimated maximum heating point for an undershoot trajectory. This establishes the maximum instantaneous heating the TPS should encounter and aids in selection of the appropriate TPS material. Seven points from an overshoot trajectory are then examined to establish the temporal variation in heating and the integrated heat load which is used to specify the TPS thickness. Afterbody heating is examined through a combination of computational predictions and experimental measurements. Finally, statistical six degree-of-freedom trajectory simulations are combined with experimental and computational heating predictions to establish the effect of angle-of-attack on heating and overall heat load.

Microprobe Geometry

The forebody geometry for Mars Microprobe is geometrically similar to that used for the small probes in the 1978 Pioneer-Venus mission[2]. It is a 45-degree half-angle sphere-cone with nose radius equal to half the base radius. The shoulder radius is one tenth the nose radius. For Microprobe, the base radius is 0.175 m, the nose radius is 0.0875 m and the shoulder radius

*Aerospace Engineer, Aerothermodynamics Branch, Aero- and Gas-Dynamics Division, NASA Langley Research Center, Senior member AIAA.
†Aerospace Engineer, Aerothermodynamics Branch, Aero- and Gas-Dynamics Division, NASA Langley Research Center, Senior member AIAA.
‡Aerospace Engineer, Aerothermodynamics Branch, Aero- and Gas-Dynamics Division, NASA Langley Research Center, Senior member AIAA.
§Aerospace Engineer, Vehicle Analysis Branch, Space Systems and Concepts Division, NASA Langley Research Center, Member AIAA.

is 0.00875 m.

The aeroshell geometry is shown in Fig. 1. The afterbody is hemispherical with radius at the center-of-gravity location. This hemispherical afterbody shape is much larger than that used on the Pioneer Venus probes. Selection of the aeroshell is discussed in Ref. 3.

Entry Trajectories

Predicting heating on the Microprobe aeroshells during their entry at Mars requires knowledge of the expected entry trajectory. Six degree-of-freedom (6-DOF) entry trajectory simulations were performed using the Program to Optimize Simulated Trajectories (POST)[4] with an aerodynamic database comprised of free molecular, Direct Simulation Monte Carlo calculations, CFD calculations, wind tunnel data, and ballistic range data. The creation of the aerodynamic database is discussed in Ref. 3. Velocity at atmospheric interface is assumed to be 6.90 km/s. The nominal inertial entry angle (γ) is -13.25 deg at radius of 3522.2 km.

With respect to heating, the major uncertainties in the trajectory simulation are the entry angle at atmospheric interface and the vehicle mass. For heatshield design, the vehicle mass is assumed to be 3.84 kg which represents a ballistic coefficient of 38 kg/m^2. (Nominal mass is 3.405 kg for a ballistic coefficient of 33.7 kg/m^2.) The uncertainty in the entry angle is plus or minus 0.4 degrees. Thus, in addition to a nominal trajectory, undershoot and overshoot trajectories are predicted by POST with entry angles of -13.65 and -12.85 degs respectively.

Stagnation point heating to a sphere can be estimated from a Sutton-Graves predictor[5]. The Sutton-Graves correlation for the Mars atmosphere (97 percent CO_2 and 3 percent N_2 mass fractions) at this direct entry condition is;

$$q_s = 1.89 \times 10^{-8} R_n^{-0.5} \rho_\infty^{0.5} V_\infty^3 \qquad (1)$$

where R_n is the radius in m; ρ_∞, V_∞ are the free-stream density and velocity in kg/m^3 and m/s; and q_s is in W/cm^2. Heating estimates for the three trajectories using nose radius as the radius in this relation are plotted in Fig. 2. (Time zero is the atmospheric interface initiation of the simulations.) The maximum heat rate expected for Microprobe occurs around t = 78.9 s for the undershoot trajectory. The conditions associated with this point are given in Table 1 and will be examined in detail using CFD. Maximum integrated heat load for Microprobe occurs for the overshoot trajectory. Seven points are examined in detail for this trajectory. Those trajectory points are indicated in Fig. 2 and listed in Table 2.

Since Microprobe encounters the Mars atmosphere while tumbling, its attitude at atmospheric interface is unknown. The three reference trajectories discussed above assume the vehicle is at zero degrees angle-of-attack. If the vehicle encounters the atmosphere while traveling at some other attitude, for example backwards, the aeroshells will reorient themselves forward but non-zero angles-of-attack oscillations may persist through some part of the heat pulse. It is necessary to assess the impact of these non-zero angle-of-attack attitudes on heating. To accomplish this, a statistical set of 6-DOF trajectory simulations are computed by varying the initial attitude over its expected range of values. Discussion of these trajectories and how a combination of computational and experimental results are used to accomplish this objective are included in the *Results* section.

Table 1. Maximum heating point (Undershoot trajectory).

t, s	Alt., km	M	V, m/s	$\rho, kg/m^3$
78.9	46.2	30.3	5942.8	1.9257e-04

Table 2. Overshoot trajectory points.

t, s	Alt., km	M	V, m/s	$\rho, kg/m^3$
51.7	76.7	36.2	6908.7	3.882e-06
65.6	63.7	35.0	6809.6	2.032e-05
74.6	56.5	33.7	6614.7	5.099e-05
87.5	47.9	30.4	5956.3	1.549e-04
99.6	41.9	24.6	4864.4	3.263e-04
107.5	39.0	20.4	4053.7	4.665e-04
118.4	35.8	15.2	3054.8	6.695e-04

Computational Method

The Langley Aerothermodynamics Upwind Relaxation Algorithm (LAURA) CFD code was used to predict the heating on Microprobe. LAURA is an upwind-biased, point-implicit relaxation algorithm[6] for obtaining the numerical solution to the Navier-Stokes equations for three-dimensional viscous hypersonic flows in thermochemical nonequilibrium. The Mars atmosphere version of the code[7] contains an 8-species $CO_2 - N_2$ chemical-kinetics model. This is the same computational code used to make aerodynamic and heating predictions for Mars Pathfinder[8–11]. Aerodynamic predictions from the code have agreed well with Viking flight data[11] and been shown to be in excellent agreement with Mars Pathfinder flight data[12].

Non-ablating, fully-catalytic-wall boundary conditions at radiative equilibrium wall temperatures are used in the present study.

Computational grids for the axisymmetric forebody solutions included 30 cells along the forebody and 64 cells normal to the wall with the first cell off the wall spaced so that the cell Reynolds number is 1. A comparison to a grid with twice as many points in each direction is included in the *Results* section. The afterbody axisymmetric calculation utilized a 160 x 64 grid. The three-dimensional forebody calculations used a surface mesh of 59 by 28 cells with 64 cells normal to the wall.

Mach 6 Air Heating Measurements

In an effort to assess the shoulder region and near afterbody heating rates and heat loads associated with large angles-of-attack, wind tunnel tests were conducted in the Langley 20-Inch Mach 6 Air Tunnel at NASA's Langley Research Center. The objective of the tests was to provide qualitative information on the variation of heating distribution over a large range of angles-of-attack.

The facility is a blow down wind tunnel that uses dry air as the test gas. The air can be heated to a maximum temperature of 1088^0 R by an electrical resistance heater, and the maximum reservoir pressure is 525 psi. A fixed-geometry, two-dimensional, contoured nozzle with parallel side walls expands the flow to Mach 6 at the 20-inch square test section. This tunnel is capable of injecting heat-transfer models from a sheltered position to the nozzle centerline in less than 0.6 s. The run time for this facility varies from 2 to 10 mins. A description of the facility and calibration results are presented in Ref. 13.

Table 3 presents the conditions for the Microprobe tests measured about a 4 inch diameter fused silica quartz ceramic model. The model was attached to the sting in such a way as to minimize sting interference effects over the angle-of-attack range from 0 to 45 degrees.

Table 3. Free stream conditions for Mach 6 Air Heating Measurements.

T, K	M	V, m/s	$\rho, kg/m^3$	Re_∞/ft
62.7	5.97	948.0	6.241e-02	4.3e+06

The relative-intensity two-color thermographic phosphor technique[14] was used to measure surface heat transfer to the model. When illuminated with ultraviolet light, electrons within the phosphor coating are excited and emit visible light during their subsequent relaxation to lower energy levels. The probability that this relaxation occurs is temperature dependent. A true-color-separation camera is used to record the emissions from which quantitative temperature information and thus heat transfer can be determined. The camera was positioned to view the wind side of the model's forebody and afterbody when at angle-of-attack.

The validity of using Mach 6 air measurements to provide qualitative information about the heating distribution on a vehicle traveling Mach 30 in Mars's CO_2 atmosphere is uncertain. A comparison with CFD prediction at zero angle-of-attack is included in the *Results* section.

Results

Computational solutions at zero-degree angle-of-attack for the undershoot and overshoot trajectories are presented first. An assessment of afterbody heating is next, followed by a discussion of angle-of-attack effects. The experimental measurements are included in the discussions of afterbody heating and angle-of-attack effects.

Maximum Heating

Figure 3 presents the laminar, zero angle-of-attack, forebody heating predicted at the undershoot trajectory's maximum heating point (Table 1) with a 30 × 64 grid and a 60 × 128 grid. In the figure, s is the distance along the body from the stagnation point. Good agreement is observed between the predictions from the two grids. The stagnation point heating prediction is 194 W/cm^2 on the finer grid which is 3.6 percent higher than the approximation from Eqn. 1. The prediction for the 30 × 64 grid agrees with the finer grid prediction except it is 2 percent lower at the stagnation point.

Heating on the forebody conical flank is about half the stagnation point value. There is no appreciable rise in heating predicted on the shoulder. Radiative heating is estimated, using the Tauber-Sutton[15] method, to be less than one percent of the convective heating presented. It can therefore be neglected in sizing the heatshield. Figure 4 presents the forebody pressure distribution associated with the two calculations. The stagnation point pressure is 0.064 atm. Maximum stagnation point pressure occurs at t= 91.5 s in the undershoot trajectory with a value of 0.094 atm.

An independent check on the stagnation point maximum heating was performed by using a Mars atmosphere version of the Viscous Shock Layer (VSL) code[16]. This method accounts for thermochemical nonequilibrium conditions in the shock layer and includes a 16 species kinetics model of which the 8 species model used in LAURA is a subset. The additional species allow for ionization. The wall temperature is set to its radiative equilibrium value and

recombination at the surface is assumed to return the mixture to its equilibrium composition at the wall pressure and temperature. This method predicts stagnation point heating (non-ablating) at 178 W/cm^2 with no appreciable ionization. This prediction is 7 percent lower than the LAURA prediction. The lower VSL prediction results from a lesser degree of wall recombination predicted by the equilibrium assumption at the wall. Temperature at the wall is 2485 K which results in a CO_2 mass fraction of 0.48 relative to the 0.97 value associated with the fully-catalytic wall LAURA solution.

All heating predictions presented assume laminar flow. The free-stream flight Reynolds number based on Microprobe's diameter is near 80,000 at maximum heating. Its maximum value is around 100,000. For Mars Pathfinder, a conservative value of 900,000 was selected as the transition flight Reynolds number[10]. Based on Reynolds number effects, therefore, the forebody boundary layer should remain laminar. In addition, the mass blowing rates due to ablation are small and the heatshield material SIRCA/Split remains smooth during ablation so that heating augmentation due to transition-to-turbulence should not occur on the Microprobe forebody.

Undershoot Trajectory Heating Predictions

Computational heating predictions for the seven trajectory points listed in Table 2 are presented in Fig. 5. The calculations were computed on 30 × 64 grids. The maximum heating for this trajectory is 175.9 W/cm^2 at t = 87.5 s. Figure 6 compares the stagnation point values from the seven solutions to the approximation of Eqn. 1. The approximation is about 11 percent lower than the CFD predictions prior to the maximum heating, and is approximately 18 percent above the CFD predictions after maximum heating. The integrated heat load from the approximation is 8712 J/cm^2. An estimate of the integrated heat load from the CFD solutions computed by fitting a similarly shaped curve through the points is 8860 J/cm^2.

Trajectory points prior to t = 51.7 s cannot be reliably predicted with continuum CFD methods like LAURA. The Knudsen number associated with the 51.7 s trajectory point is 0.06.

Afterbody Heating

A zero angle-of-attack CFD solution was generated about the full vehicle to estimate heating on Microprobe's hemispherical afterbody. This calculation was performed at the maximum heating point from an undershoot trajectory and used the 160 by 64 grid shown in Fig. 7 (64 points normal to the surface). Figure 8 presents the predicted heating for the forebody and the afterbody. Figure 9 details the afterbody prediction. Heating drops rapidly around the shoulder to around one percent of the forebody stagnation point value. The flow stays attached along most of the afterbody. Additional discussion of afterbody heating is contained in the next section.

Angle-of-Attack Effects

Because the Mars Microprobe may encounter the atmosphere of Mars at an uncertain orientation, the envelope of possible angles-of-attack early in the trajectory is large. From 6-DOF Monte-Carlo simulation, a plot of the expected total angles-of-attack as compared to the heat rates is shown in Fig. 10. At the point when stagnation point heating rate is half of its maximum, the three-sigma variation on total angle-of-attack is as large as 40 degrees. These large angles-of-attack during the heating pulse need to be accounted for in design of the probe's TPS.

Figure 11 presents the Mach 6 thermographic phosphor measurements in the form of a heat transfer coefficient (Ch) normalized to the zero degree angle-of-attack stagnation point value (Ch_{ref}). The measurements were taken only on the windside of the vehicle. The measurements reveal that windside shoulder region heating ratio increases from 0.40 to 0.81 as angle-of-attack increases from zero to 45 degrees. Figure 12 shows a close-up of the afterbody region.

Figure 13 compares the measured zero angle-of-attack normalized heating distributions to LAURA CFD predictions at Mach 30 Mars conditions discussed in the *Afterbody Heating* section above. A CFD calculation for Mach 6 air (forebody-only calculation) is also included. Real gas effects are evident on the forebody frustrum where the Mars calculation predicts higher heating (relative to the stagnation point value) than both the measured values and the Mach 6 air calculation. Figure 14 presents a close-up of the afterbody region.

Figure 15 presents forebody heating across the symmetry plane (normalized to the zero angle-of-attack stagnation point value) from CFD predictions at 0, 10 and 20 degrees angle-of-attack at a trajectory point near maximum heating in the nominal trajectory. On the windside (positive x in the figure), the heating increases with angle-of-attack and the qualitative nature of the distribution changes as a result of the shift of the sonic line from the nose to the shoulder. Leeside heating (negative x) is reduced with increased angle-of-attack.

The motion of the Microprobe during the heat pulse is an oscillation in angle-of-attack (α) and side-slip angle (β). Figure 16 presents a representative trajectory showing the relationship between the aerodynamic angles and the heat pulse. To predict the expected maximum heating rate and heat load which the heatshield must be designed for, the information in Figs. 11, 15, and 16 can be combined. To make the problem tractable, seven points are selected on the Microprobe geometry as shown in Fig. 17. Windside heating predictions in Figs. 11 and 15 as well as leeside predictions

in Fig. 15 are used to estimate the heating at each of the seven points as a function of angle-of-attack. The actual motions from the trajectory in Fig. 16 can then be used to integrate the heat load at each of the points. (To assess heating for non-zero azimuthal points, a sinusoidal variation from windside to leeside is assumed.) The predicted heating at each of the points is given in Fig. 18 for the trajectory shown in Fig 16. By repeating this methodology for all possible entry trajectories from a 6-DOF Monte-Carlo entry simulations, a statistical examination of the effect of angle-of-attack (as well as other off-nominal conditions simulated in the 6-DOF) on heating at each of the 7 points can be conducted. A Summary of the results of this calculation are given in Table 4 for heat rate and Table 5 for heat load.

Table 4. Maximum heat transfer rate (in W/cm^2) at 7 Points on the body from 6-DOF Monte-Carlo analysis (with angle-of-attack effects).

point	Min	Mean	Max	3-σ Dev.
1	166.3	178.8	201.8	13.3
2	100.6	112.4	130.7	11.4
3	83.3	93.2	108.6	9.45
4	79.2	87.1	100.7	7.88
5	9.76	11.66	16.0	2.28
6	1.67	2.75	7.15	3.3
7	3.34	3.69	6.05	0.94

Table 5. Integrated heat load (in J/cm^2) at 7 points on the body from 6-DOF Monte-Carlo analysis (with angle-of-attack effects).

point	Min	Mean	Max	3-σ Dev.
1	7327	8112	8816	517
2	4130	4571	5003	306
3	3314	3706	4102	281
4	3217	3589	3943	247
5	438	509	595	91
6	82	103	147	36
7	164	193	244	46

While the methodology used to generate tables 4 and 5 is valid, the accuracy of the values presented in the tables is limited by the accuracy of the data used to establish the effect of angle-of-attack on heating distributions around the probe. In particular, the large angle-of-attack variation relies heavily on the Mach 6 air experimental measurements whose applicability to this higher speed Mars entry is uncertain. In addition, leeside heating on the afterbody and azimuthal variations had to be estimated. The accuracy could be increased through a series of computationally-expensive CFD calculations (including the wake) for the entire range of angles-of-attack.

Traditionally, planetary entry heatshield design utilized the maximum heat rate from the undershoot trajectory and the heat load from the overshoot trajectory while neglecting off-nominal angle-of-attack effects as well as other off-nominal conditions typically included in 6-DOF Monte-Carlo trajectory analysis. (Off-nominal conditions examined are discussed in Ref. 4.) To assess the effect of these off-nominal conditions, the 3-σ values from Tables 4 and 5 (mean value plus 3-σ deviation) can be compared with values predicted from traditional heatshield sizing approaches. This comparison, in the form of ratios of the 3-σ 6-DOF values to the traditional value for both heat rate and heat load to each of the 7 body points, is given in Table 6.

Table 6. Ratios of Angle-of-Attack Effects to Zero angle-of-attack (Mean Trajectory).

point	Max. Rate	Heat Load
1	0.99	0.97
2	1.10	0.95
3	1.10	0.94
4	1.07	0.94
5	1.44	1.35
6	3.12	1.57
7	1.19	1.35

This table reveals that the effect of angle-of-attack and other off-nominal conditions increases the maximum heat rate predicted on much of the forebody by about 10 percent (except at the stagnation point) while decreasing the heat load to the forebody by 3-6 percent. On the afterbody, the heat rates can be as much as a factor of 3 higher with the associated heat loads increased by 30-60 percent.

Conclusions

Design of an efficient TPS for Mars Microprobes requires prediction of the expected aerothermal heating which the aeroshells will encounter during the hypersonic portion of their trajectory. A combination of computational predictions and experimental measurements is used to provide this prediction.

The maximum instantaneous heating rate at the vehicle's stagnation point (at $\alpha = 0^0$)is predicted using the CFD code LAURA to be 194 W/cm^2. This value is 3.6 percent higher than a Sutton-Graves approxi-

mation and is 7 percent higher than a VSL prediction. No significant heating augmentation due to radiation is expected. The forebody shock layer should remain laminar. Maximum stagnation point pressure expected is 0.094 atm.

From computations at seven overshoot trajectory points (ballistic coefficient = 38 kg/m^2), the maximum heat load expected at the stagnation point is estimated to be 8800 J/cm^2.

Heat rates and heat loads on the vehicle's afterbody are much lower than the forebody. At zero degree angle-of-attack, heating over much of the hemispherical afterbody is predicted to be less than 2 percent of the stagnation point value.

Good qualitative agreement is demonstrated for zero angle-of-attack afterbody heating between CFD calculations at Mars entry conditions and experimental thermographic phosphor measurements from the Langley 20-Inch Mach 6 Air Tunnel. On the forebody frustrum, the experimental data is as much as 30 percent lower than the Mars-atmosphere CFD prediction.

The effect of angle-of-attack and other off-nominal conditions increases the maximum heat rate encountered on much of the forebody by about 10 percent while decreasing the heat load to that region by 3-6 percent. Angle-of-attack increases afterbody heating as much as a factor of 3 with associated heat loads increased by 30-60 percent.

Acknowledgments

Thanks are extended to Dr. Roop Gupta of NASA Langley Research Center for supplying the VSL heating estimate and Mr. Eric Slimko of the Jet Propulsion Laboratory for many helpful discussions.

References

[1]Powell, G., and Gavit, S., "New Millennium Mars Microprobe Mission and System Specifications," NMP/Spec-02, JPL-D-13752, Sept., 1996.

[2]Weinberg, S. A.,"Final Data Report - Pioneer-Venus Static and Dynamic Transonic Wind Tunnel Tests," 9154-TDM-75-013, General Electric Corp, July 11, 1975.

[3]Mitcheltree, R. A., Moss, J. N., Cheatwood, F. M., Greene, F. A., and Braun, R. D., "Aerodynamics of the Mars Microprobe Entry Vehicles," AIAA Paper No. 97-3658, Aug., 1997.

[4]Braun, R. D., Mitcheltree, R. A., and Cheatwood, F. M.,"Mars Microprobe Entry Analysis," *Proceedings from the 1997 IEEE Aerospace Conference*, Feb. 1997.

[5]Sutton, K., Graves, R. A.,"A General Stagnation-Point Convective-Heating Equation for Arbitrary Gas Mixtures," NASA TR R-376, Nov., 1971.

[6]Gnoffo, P. A.,"An Upwind-Biased, Point-Implicit Relaxation Algorithm for Viscous, Compressible Perfect-Gas Flows," NASA TP-2953, Feb. 1990.

[7]Mitcheltree, R. A.,"Aerothermodynamic Methods for a Mars Environmental Survey Mars Entry," *Journal of Spacecraft and Rockets*, Vol. 31, No. 3, May-June, 1994, pp. 516-523.

[8]Braun, R. D., Powell, R. W., Engelund, W. C., Gnoffo, P. A., Weilmuenster, K. J., and Mitcheltree, R. A.,"Mars Pathfinder Six-Degree-of-Freedom Entry Analysis," *Journal of Spacecraft and Rockets*, Vol. 32, No. 6., Nov-Dec., 1996, pp. 993-1000.

[9]Mitcheltree, R. A., Gnoffo, P. A., "Wake Flow About the Mars Pathfinder Entry Vehicle," *Journal of Spacecraft and Rockets*, Vol 32., No. 5., Sept.-Oct., 1995, pp. 771-776.

[10]Mitcheltree, R. A., "Computational Aerothermodynamics For Mars Pathfinder Including Turbulence," AIAA Paper 95-3493, Aug. 1995.

[11]Gnoffo, P. A., Weilmuenster, K. J., Braun, R. D., and Cruz, C. I., " Influence of Sonic Line Location on Mars Pathfinder Aerodynamics," *Journal of Spacecraft and Rockets*, Vol. 33, No. 2, Mar-Apr. 1996, pp. 169-177.

[12]Gnoffo, P. A., Weilmuenster, K. J., Powell, R. W., Mitcheltree, R. A., Engelund, R. D., and Braun, R. D., "Prediction ad Validation of Mars Pathfinder Hypersonic Aerodynamic Data Base," to be presented at the 7th AIAA/ASME Joint Thermophysics and Heat Transfer Conference, June 1998.

[13]Micol, J. R., "Hypersonic Aerodynamic/Aerothermodynamic Testing Capabilities at Langley Research Center: Aerothermodynamic Facilities Complex," AIAA Paper No. 95-2107, Jun., 1995.

[14]Merski, N. R.,"A Relative-Intensity Two-Color Phosphor Thermography System," NASA TM 104123, 1991.

[15]Tauber, M. E., and Sutton, K.,"Stagnation-Point Heating Relations for Earth and Mars Entries," *Journal of Spacecraft and Rockets*, Vol. 28, No. 1, Jan.-Feb., 1991, pp. 40-42.

[16]Gupta, R. N., Lee, K. P., Moss, J. N., and Sutton, K.,"Viscous Shock Layer Analysis of the Martian Aerothermal Environment," *Journal of Spacecraft and Rockets*, Vol. 29, No. 5, Sept.-Oct., 1992, pp. 663-640.

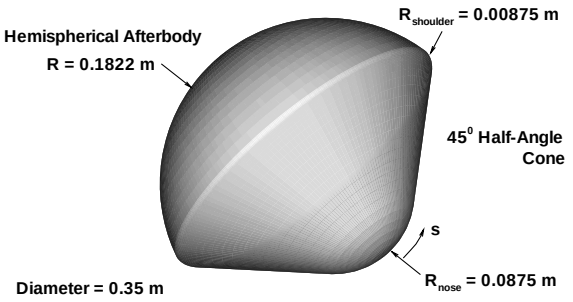

Fig. 1 Geometry of Microprobe aeroshell.

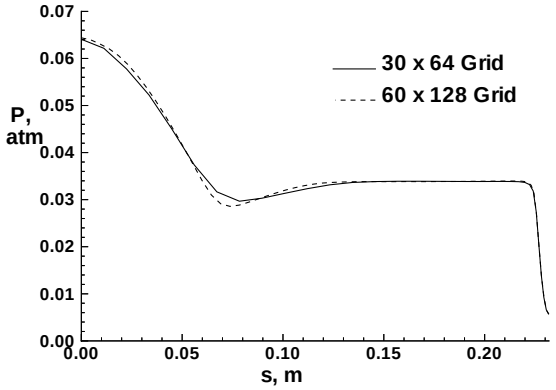

Fig. 4 Forebody pressure distribution for maximum heating point on undershoot trajectory.

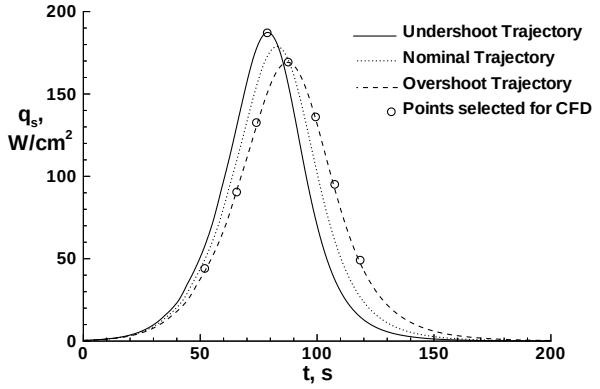

Fig. 2 Sutton-Graves stagnation point heating estimate for heatshield design trajectories with B=38 kg/m^2.

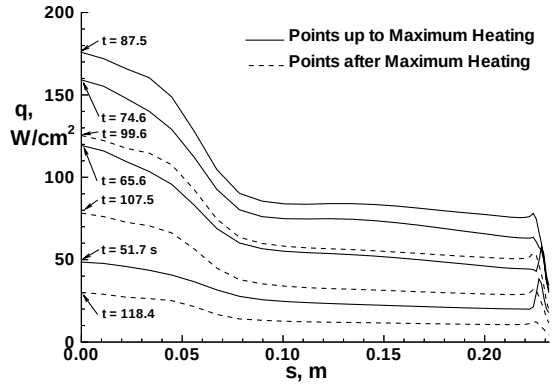

Fig. 5 Forebody heating distributions for seven overshoot trajectory points.

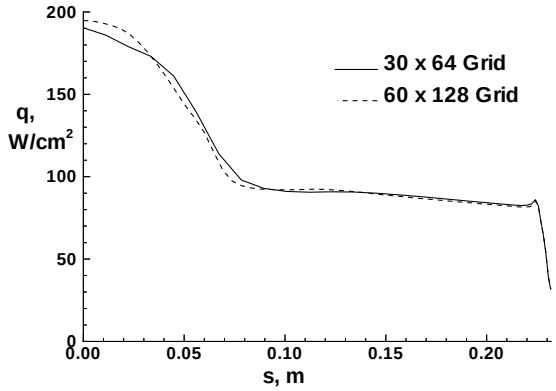

Fig. 3 Forebody heating distribution for maximum heating point on undershoot trajectory.

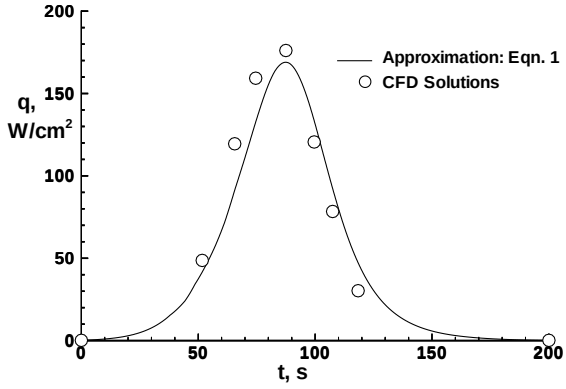

Fig. 6 Comparison of stagnation point heating from CFD predictions to the approximation of Eqn. 1 for the overshoot trajectory.

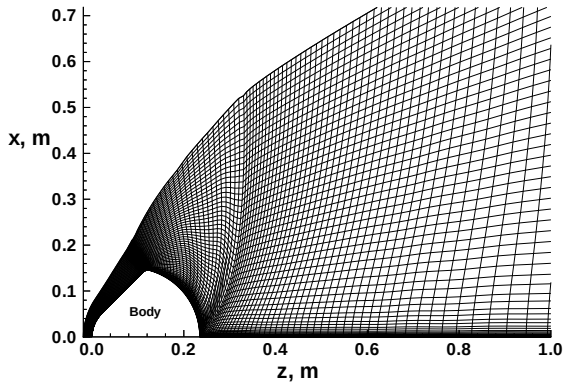

Fig. 7 160 x 64 full vehicle axisymmetric computational grid.

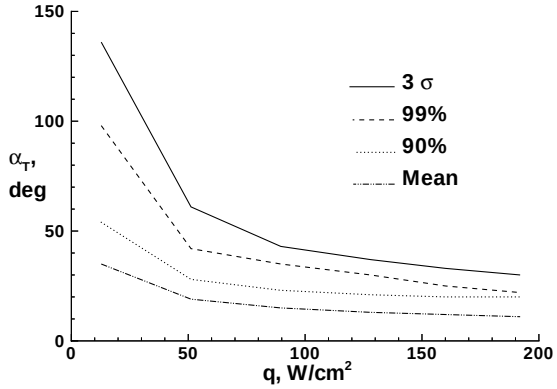

Fig. 10 Statistical variation in total angle-of-attack as a function of stagnation point heat rate.

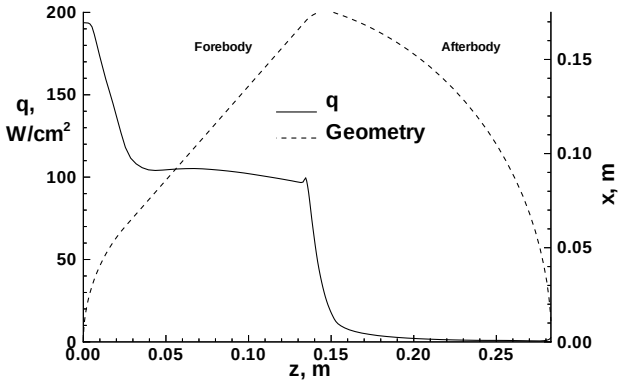

Fig. 8 Forebody and afterbody heating distributions for a maximum heating point in an undershoot trajectory.

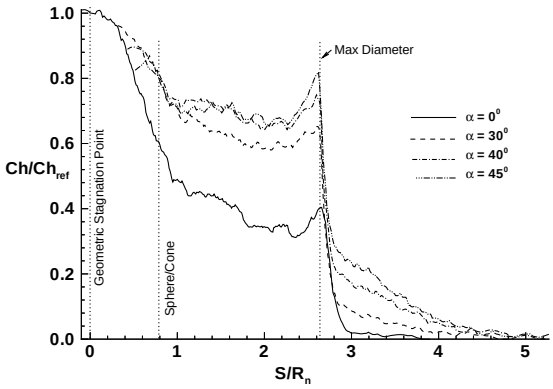

Fig. 11 Thermographic phosphor measurements of normalized heat transfer coefficient from Langley 20-Inch Mach 6 Air Tunnel (Re/ft = **4.3** $\times 10^6$).

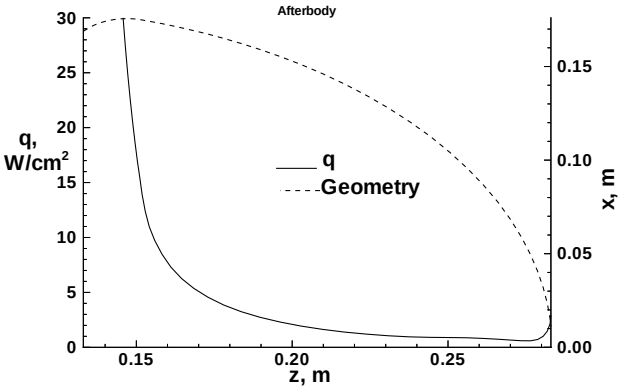

Fig. 9 Close-up of afterbody heating distributions for a maximum heating point in an undershoot trajectory.

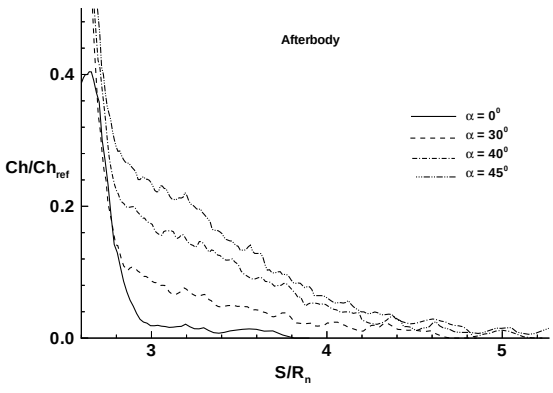

Fig. 12 Afterbody thermographic phosphor measurements of normalized heat transfer coefficient from Langley 20-Inch Mach 6 Air Tunnel (Re/ft = **4.3** $\times 10^6$).

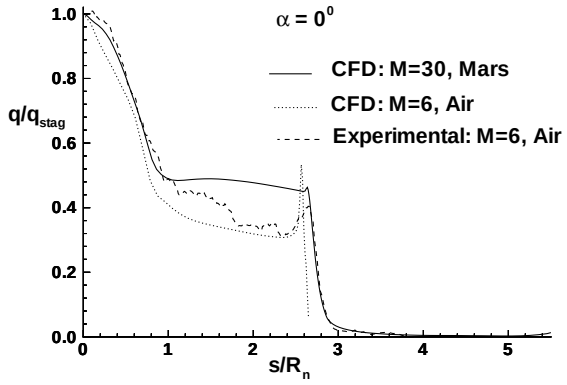

Fig. 13 Comparison of normalized heating predictions from CFD at Mach 30 in Mars atmosphere, perfect gas CFD at Mach 6 in air, and measurements at Mach 6 in air.

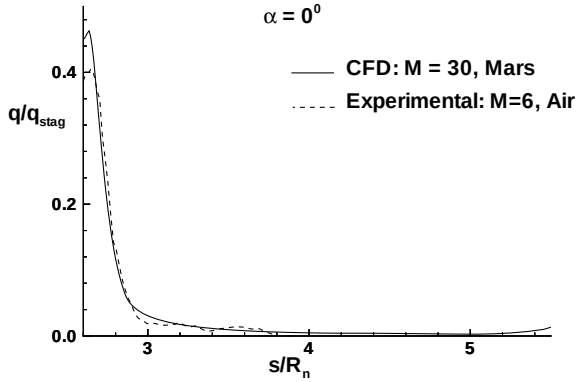

Fig. 14 Comparison of normalized afterbody heating predictions from CFD at Mach 30 in Mars atmosphere with measurements at Mach 6 in air.

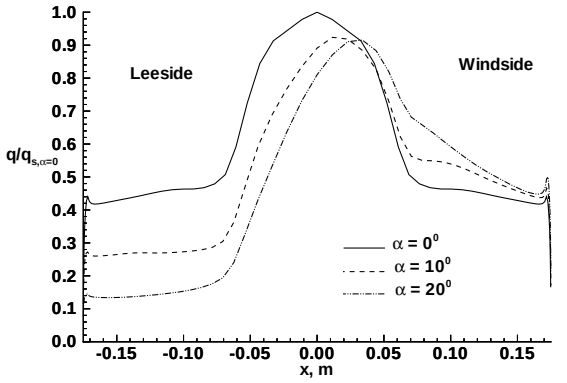

Fig. 15 Effect of angle-of-attack on normalized forebody heating across the symmetry plane from CFD predictions (Mars atmosphere).

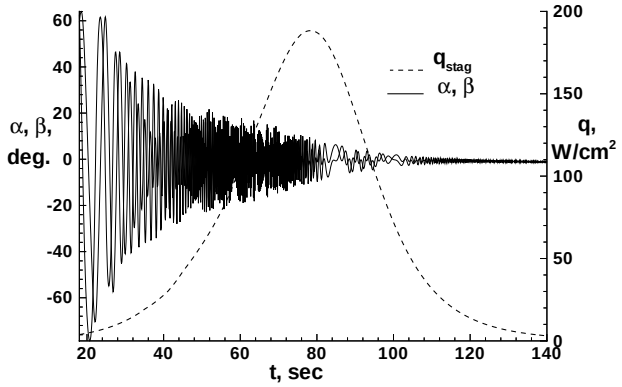

Fig. 16 Relationship between vehicle attitude angles and the heat pulse for one possible trajectory.

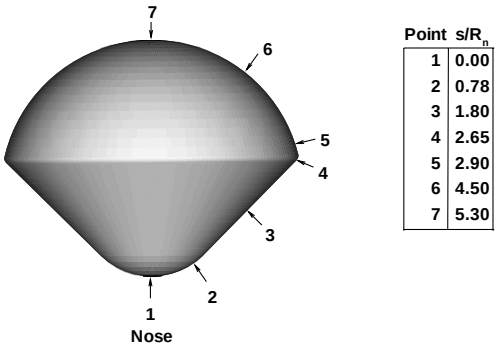

Point	s/R_n
1	0.00
2	0.78
3	1.80
4	2.65
5	2.90
6	4.50
7	5.30

Fig. 17 Definition of seven selected points on Vehicle for 6-DOF heating tracking.

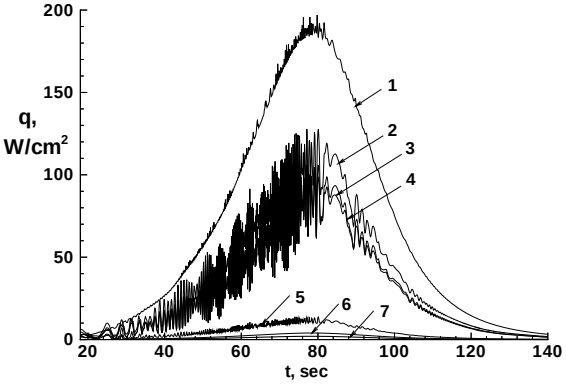

Fig. 18 Time history of heating at seven selected points on geometry for one possible trajectory.